SHAFT PREMATURE FAILURE ANALYSIS IN ELECTRICAL SUBMERSIBLE PUMP SYSTEM: A CASE STUDY FROM MUARA ENIM, SOUTH SUMATERA, INDONESIA

Diah Kusuma Pratiwi*, Yudianto, Agung Mataram, Akbar Teguh Prakoso

Department of Mechanical Engineering, Faculty of Engineering, Unviersitas Sriwijaya, Ogan Ilir – 30662, South Sumatera, Indonesia

ABSTRACT

The shaft is a critical component in ESP. In many cases, dismantle analyses cannot identify a definitive root cause for shaft failure. Several hypotheses have been studied to explain shaft failure. This paper will review typical shaft failure modes; more specifically, the power source and the consequence of shaft failure will be discussed. An analysis of the premature failure of the shaft used in an electrical submersible pump (ESP) for lifting oil has been carried out. During shaft failure root-cause analysis, mechanical components have been the primary focus. Chemical analysis, microstructure characterization, fractography, and hardness test were used. In addition, the shaft running stress and the possibility condition (the condition of the possible broken shaft has been approached analysis using finite element analysis). It was concluded that the material defects were the prime cause of the shafts' premature failure.

Keywords: Failure, Submersible Pump System, Shaft

1 INTRODUCTION

An Electric Submersible Pump (ESP) is an artificial lift technique commonly used for oil and gas recovery from downhole reservoirs. It consists of multi-stage rotating impeller blades driven by medium voltage electric submersible AC motors. The pump-motor assembly in an ESP system is placed inside a downhole well, located hundreds to several thousands of meters below the surface. While spinning, the pump blades increase the pressure of the reservoir fluid and force it to reach the surface. The oil recovery rate depends on the pressure produced by the ESP and is adjustable by varying the speed of the motor. Thus, ESPs can achieve a wide rate of production ranging from 200 to over 20,000 barrels of fluids per day [1]. Since the inception of ESPs, three-phase squirrel-cage induction submersible motors have been the de-facto technology as the prime mover. On the surface, the power supply to the submersible motor can be either a switchboard or a variable frequency drive (VFD) through a lengthy downhole cable. An ESP motor startup directly from a switchboard supply creates a large starting current, which can be 6 to 9 times the motor-rated current, and thus introduces severe mechanical stress in the system [2][3][4][5]. They expose the ESP shafts and interconnections to overload conditions and result in ESP failures [6][7][8]. Extended exposure to fluctuating mechanical stress can also introduce fatigue in the system. Another investigation of the pump shaft breakage is the bad pump assembly or the pump aging.

This case study describes the failure analysis of a premature fracture ESP shaft that led to catastrophic consequences in terms of damage to other equipment and loss of production. Failure can also be less than catastrophic if detected early enough. It may mean a state of defectiveness, a lapse in manufacturing quality control or inspection effectiveness, the use of incorrect or below specification material, unexpected in-service deterioration, or damage through poor operation or maintenance. Even in these cases, the financial consequences can be high regarding rework, repair, or remediation. The primary objective of a material's failure analysis is to determine the root cause of failure. Whether dealing with metallic or non-metallic materials, the root cause can normally be assigned to one of four categories; i.e., design, manufacturing, service, or material.

*Corresponding author's email: pratiwidiahkusuma@ft.unsri.ac.id

Finally, the paper documents the results of an initial examination and detailed investigations. It also discussed the potential root causes of failure in the ESP shaft and the primary mode of failure. The failure analysis result includes recommendations for design improvements to the ESP system. If implemented, these recommendations should circumvent the possibility of failure of future ESP shaft systems.

2 MATERIAL AND METHOD

Information on the technical specification of the equipment, the service history, and its mode of operation will be needed for comparison with forensic evidence from the failed parts to determine the root cause of the failure. Such a comparison may indicate a cause of failure. Was the intended material used? Was the equipment operated correctly? Secondly, the context of the failure must be determined. A site visit to examine and photograph the damaged equipment is often helpful and sometimes essential. It may not be possible to recreate the scene again. What was happening at the time leading to the first sign of failure and afterward? The value of witness statements should not be underestimated; even when an eyewitness account may not be sufficiently robust for a court of law, it may provide valuable pointers to investigators.

Figure 1 shows the oil field's geographic location and daily production. This well is an "R" reservoir producer and can produce at least 1000 bbls/day. The failed component in the case study was a shaft from the pump UT unit. Typical configuration of ESP system as shown Figure 2. From the information of engineering staff, the failed shaft was made of Monel K500 and was only in service for below one week before experiencing these failures, which raised the loss of production at the oil company.

Figure 1 Case study location Map

A though background investigation was conducted to identify possible contributing factors to failure. Several important facts were uncovered during this process that will be highlighted in detail in the following sections. The ESP is a new installation using motor 120 HP/1295V/59 A. The ESP has been successfully running at 50 Hz for four days. After four days of working conditions, the ESP underwent an unplanned shutdown. The ESP failed to starting-up under normal and reverse conditions. Then the ESP starts up directly from a switchboard (60Hz), and the cable and electric motor are short. The service rig was conducted by replacing the cable and electric motor (160HP/2185V/46 A). The ESP was back to normal running condition with a frequency of 50Hz. After two days of working conditions, the ESP returned to an unplanned shutdown. The ESP failed to starting-up under normal and reverse conditions. The ESP starting-up again directly from a switchboard (60Hz), and finally shaft broke.

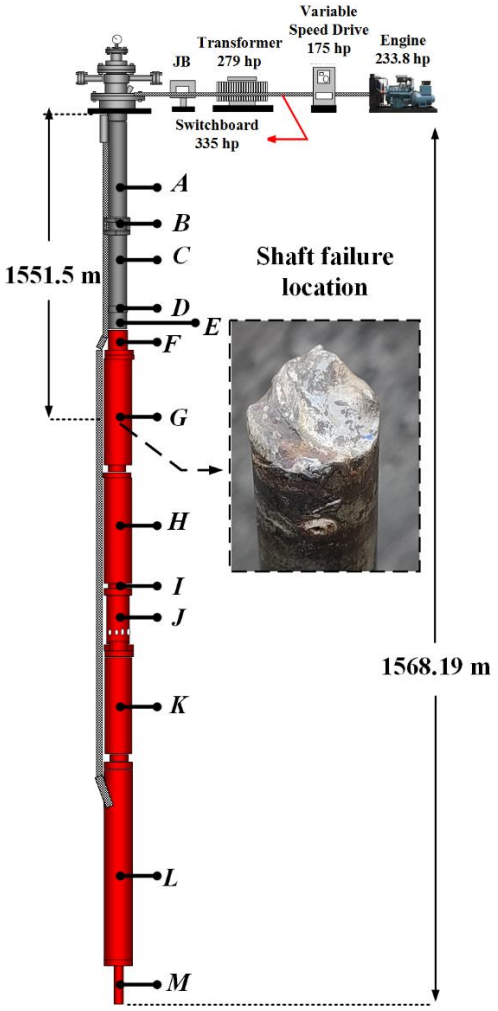

Figure 2 A typical configuration of an ESP System

Abbrev	Item	Length (m)
A	Tubing	1520.099
B	Bleeder valve	0.149
C	1st joint tubing	9.501
D	Check valve	0.149
E	2nd joint tubing	19.001
F	BOH (Bolt on head)	0.152
G	Pump UT	3.194
H	Pump LT	3.650
I	Adaptor	0.100
J	Intake gas separator	1.080
K	Protector	2.740
L	Motor	7.673
M	ESP Centralizer	0.701

The primary objective of this investigation was to evaluate the shaft material and describe its failure mode. A detailed background study was performed to understand the material and problem fully. This investigation examined the damaged parts and failure surfaces (see Fig 2). The required close attention to detail and meticulous record keeping. The initial examination included photography and a dimensional check. There would be no opportunity to return later once the component was cut up and pieces removed. Once this on-site examination was complete, samples of material were extracted for detailed laboratory examination, microstructural analysis, chemical analysis, mechanical testing, and stress analysis using the finite element approach.

3 RESULTS AND DISCUSSIONS

3.1 Visual Inspection and Fractography

The fracture morphology observation of the shaft part removed from the ESP component can be shown in figure 3. A crack started from the origin region (yellow marks) because there was no plastic deformation on the surface. Due to torsion load, the crack may occur by a defect or micro-void shear localization process/micro-void mechanism [9]. The curved concentric lines (beach marks), which indicate fatigue during the work cycle around the fracture surface, were not found. Adjacent to the fracture surface, the shaft was fully twisted (red arrow), and the fracture was perpendicular to the axis of the shaft. It may be concluded that fracture morphology is associated with combining brittle (yellow marks) and ductile failure (red arrow). Additionally, a similar morphology was observed by a previous study [10] and associated with torsional overload fracture.

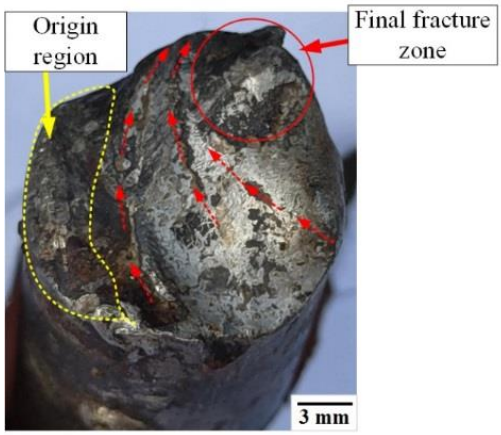

Figure 3 Evidence of failure was recovered from the ESP shaft at 1550 meters from the ground level. The fracture zone is a typical brittle and ductile fracture.

3.2 Microstructural characterization

Microstructure observation was conducted through the metallography process: sample selection, cutting, mounting, grinding, surface smoothing with sandpaper, polishing etching, and observation using an optical microscope. The specimen was mounted in epoxy resin, then ground with abrasive papers from 800 to 1500 grit for further cross-section observation. Metal polishing was using Al_2O_3 + water and followed by etching using a mixture of 50 ml HNO3 + 50 ml Acetic acid (50ml water-optional). The microstructure of the shaft material specimen was observed using HITACHI SU-1500. From the region of interest, two different microstructure of ESP shaft material has been observed revealed by using optical microscopy, as shown in Figure 5b. Firstly, the region one microstructure indicates base metals. The microstructure is Monel nickel-based alloy (Figure 5d) [11]. Regions 2 and 3, called fusion zone, indicated that columnar and equiaxed dendritic grains formed [12]. The columnar grain formed near the base metals grow perpendicular and then transforms to equiaxed grains in the center of the fusion zone—the possibility of a fusion zone formed due to the welding process. According to previous literature, Monel K-500 material is allowable to weld using the GTAW technique with filler ERNiCu-7 (FM60) [12].

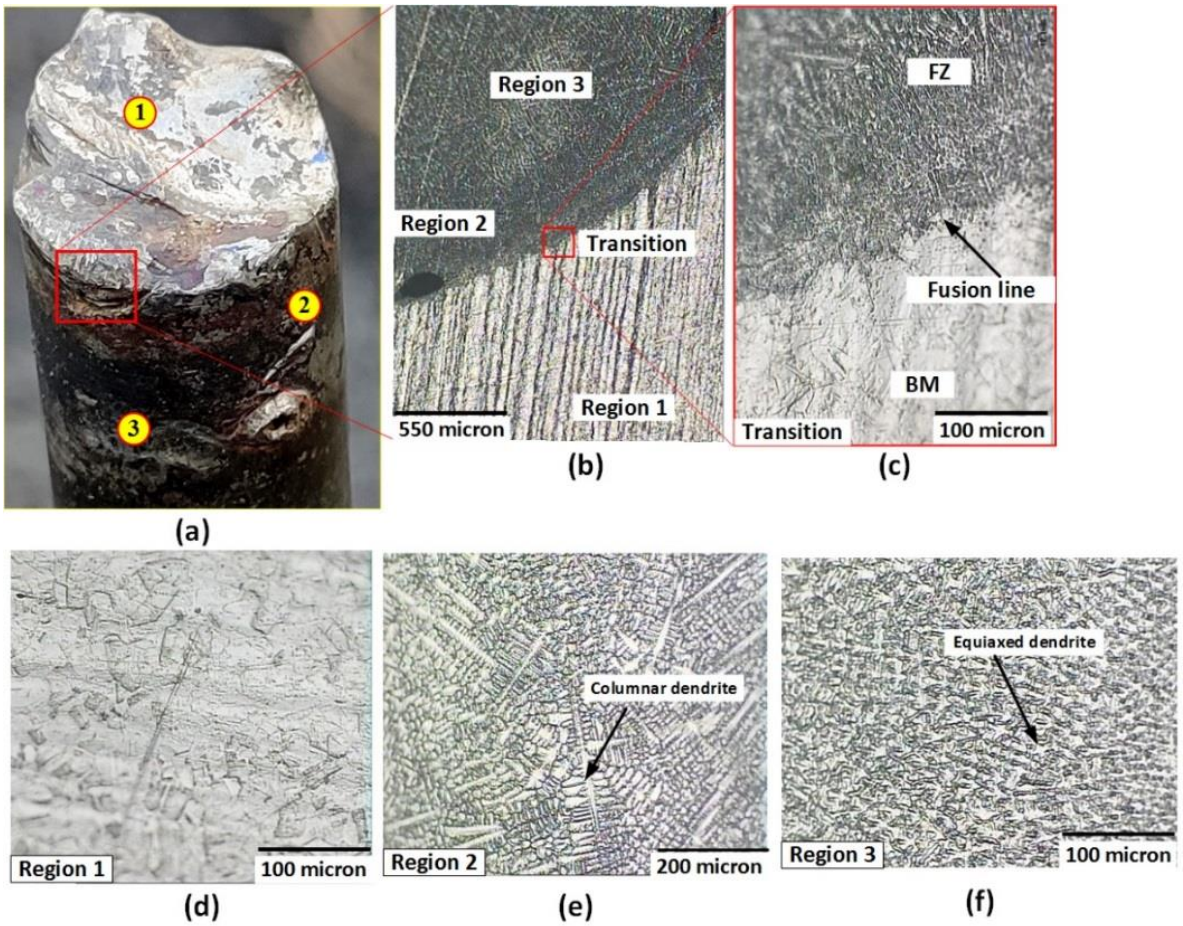

Figure 4 Macroscopic features of the shaft: (a) general view; (b) close up to the region of interest ;(c) transition; (d) Microstructure of the base metals; (e) Showing columnar dendrite at higher magnification (f) Showing equiaxed dendrite at higher magnification

3.3 Chemical Analysis

The chemical composition of the shaft was made using Thermo Scientific Niton XL2 GOLDD XRF Analyser at the location, as shown in figure 5a. Table 1 summarizes the composition analysis, revealing the alloy can be classified as a Monel K-500 nickel-based alloy, the same as previous references [13][14].

Table 1 Chemical composition analysis

Region	Ti	Mn	Fe	Ni	Cu
1	0.59	0.67	1.13	63.77	30.8
2	0.57	0.56	0.98	64.21	33.68
3	0.55	0.76	1.14	63.89	30.5

3.4 Mechanical Analysis

The mechanical properties were measured by hardness using Vickers Hardness Tester VKH-2E, based on an assessment of the indenter penetration pyramid. The sample test was prepared by cutting the sample, resin mounting, and surface smoothing with sandpaper. Macro hardness tests were performed along the shaft following JIS Z 2244 standard. The hardness test used a load of 30 kgf and was determined by using Equation 1:

$$HV = \frac{2psin\left(\frac{\theta}{2}\right)}{L^2} = 1.854\frac{P}{L^2} \quad (1)$$

We are using a conversion table according to standard ASTM E140-12b [15], the hardness of the shaft material around HBS 226-390. According to previous literature, the hardness of the shaft material from indentation locations 3 to 19 has a good agreement with Monel K-500 in the cold drawn and aged condition process according to previous literature [13]. In contrast, the hardness values at indentation locations 1 and 2 are slightly softer towards the fracture zone (fused zone) (see figure 6). Based on the result, the hardness value at locations 1 and 2 is the same with filler weld material which contains ERNiCu-7 (FM60) about 160-219 VHN [16].

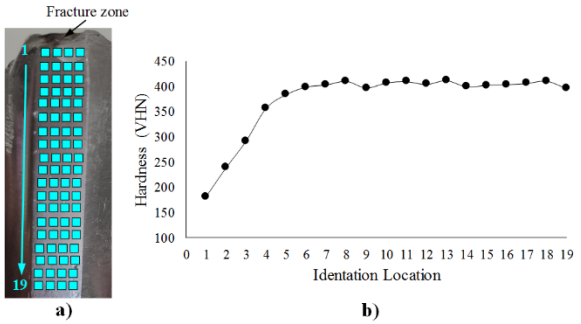

Figure 5 (a) Indentation hardness location (b) Hardness profile measured on the shaft

3.5 Stress Analysis

The finite element (FE) analysis was applied to analyze the stress distribution in the surroundings of the ESP shaft and its relation to the fracture phenomenon. To evaluate the effect of torsion load due to an electric motor on the stress distribution on the shaft. The geometry and FE analysis of the ESF shaft were conducted using Solidworks software. The diameter of the shaft is about 17,40mm. The boundary condition of this analysis is shown in Figure 7a. Torsion moments due to transmitted power from the motor to the ESP shaft are about 237 Nm and 317 Nm, respectively. The shaft mesh was generated using a tetrahedral element with linear approximation (figure 7c). The material of the shaft was assumed to be a linear elastic material. The mechanical properties of the Monel K-500 cold drawn-aged process for simulation purposes include E = 160 GPa, $\vartheta = 0.32$, $\sigma_y = 1103$ MPa, $\sigma_{ut} = 1276$ MPa [17].

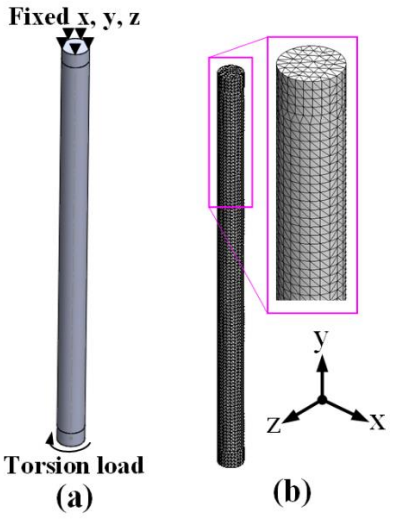

Figure 6 (a) Geometry of finite element model (b) Mesh setting

The stress results from the simulation as tabulated in Table 2. The maximum calculated von mises stress under torque 237 and 317 Nm were 402.51 MPa and 538.38 MPa, respectively, far below the material's yield strength. The safety factor of shaft material is above 1.5, and which typical safety factor would be at least 1.5 – 4 [18].

Table 2 Simulation results

Power (HP)	Torsion load (Nm)	Results			
		Analytic	Simulation		
		Shear Stress (MPa)	Shear Stress (MPa)	Von mises stress (MPa)	Safety Factor
120	237	229.24	230.53	402.51	2.74
160	317	306.62	308.35	538.38	2.04

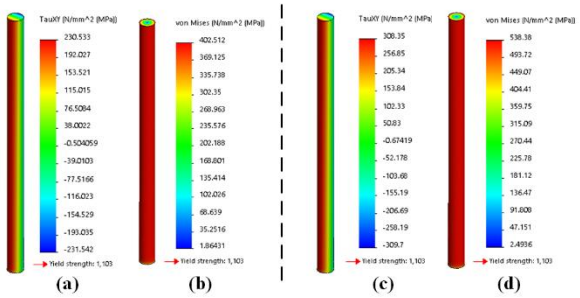

Figure 6 Stress analysis in ESP shaft; (a) shear stress under torque load of 237 Nm, (b) von mises stress under torque load of 237 Nm, (c) shear stress under torque load of 317 Nm, (d) von mises stress torque load of 317 Nm.

3.6 Final Analysis (root causes)

Based on this information, the chain of the shaft failure in the ESP system is summarized in Figure 8. However, the weld product/plugs created stress concentrations transporting the failure to the shaft. However, in shaft application, weldment should not exist. Load frequency of power is not the main cause because that's not overload. After all, finite element testing has been done. If an un-normal occurs, if the shaft occurs suddenly fixes the material.

The shaft has a defect during the manufacturing process; it is done gojing to cover the defect area. The difference in the specimen's

microstructure is there are areas of dendritic solidification structure caused by the superheated temperature. These dendritic areas are usually caused by casting and welding (are there monel dendritic areas?). In addition, the chemical composition of dendritic material is very different from that of typical monel materials. When the torque is high, the gojing material cannot withstand torsional loads, the defect area causes high-stress concentrations, and the shaft experiences ductile fracture.

It can be concluded that the specimen was superheat melted, which could be expected concerning the welding treatment. The microstructure we observed is similar to what has been reported in the literature.

So it can be said that the fracture process in the pump shaft is because of one side of the shaft. The bearing holder suddenly stops until an impact load occurs on the shaft. Hence, the condition of the motor is working to rotate the shaft so that a torsional arises. Consequently, the shaft can no longer withstand the working torsional load until deformation occurs, and finally, the shaft breaks due to overload. The fracture occurs in the weld area (gojing) defects resulting in a high-stress concentration (stress concentration).

4 CONCLUSIONS

In this study, the failure analysis of the ESP shaft is analyzed in detail. Several causes of ESP shaft failure have been analyzed and compared with the dismantle evidence. The investigation case ruled out the load-induced failure and material and (salah pasang). The material can majorly contribute to shaft failure when bronze debris is generated. After a review of all possible failure causes. After a review of all possible failure causes, the power quality-induced. Hence, it is important to create an acceptable power quality guideline for the VSD and perform the necessary testing before the system installation. This would help the operator reduce the unexpected ESP failure problem, especially for high-horsepower systems.

ACKNOWLEDGMENTS

The authors would like to convey their great appreciation to Universitas Sriwijaya for supporting this research.

REFERENCES

[1] Joel Romero O and Hupp A 2014 Subsea Electrical Submersible Pump Significance in Petroleum Offshore Production *J. Energy Resour. Technol.*

[2] Durham R A and Brinner T R 2015 Oilfield Electric Power Distribution *IEEE Trans. Ind. Appl.*

[3] Thorsen O V and Dalva M 2001 Combined electrical and mechanical model of electric submersible pumps *IEEE Trans. Ind. Appl.*

[4] Vandermeulen A H, Natali T J, Dionise T J, Paradiso G and Ameele K 2019 Exploring New and Conventional Starting Methods of Large Medium-Voltage Induction Motors on Limited kVA Sources *IEEE Transactions on Industry Applications*

[5] Ledoux K, Visser P W, Hulin J D and Nguyen H 2015 Starting large synchronous motors in weak power systems *IEEE Trans. Ind. Appl.*

[6] Pragale R and Shipp D D 2017 Investigation of Premature ESP Failures and Oil Field Harmonic Analysis *IEEE Trans. Ind. Appl.*

[7] Farbis M, Hoevenaars A H and Greenwald J L 2016 Oil field retrofit of ESPs to meet harmonic compliance *IEEE Trans. Ind. Appl.*

[8] El-Mahayni R, Al-Qahtani K and Al-Gheeth A H 2016 Large Synchronous Motor Failure Investigation: Measurements, Analysis, and Lessons Learned *IEEE Trans. Ind. Appl.*

[9] McVeigh C, Vernerey F, Liu W K, Moran B and Olson G 2007 An interactive micro-void shear localization mechanism in high strength steels *J. Mech. Phys. Solids*

[10] Sunandrio H and . S 2014 Analisis Kegagalan Shaft Pompa Submersible Pada Unit Pengeboran Minyak Bumi = Failure Analysis Of Pump Shaft Submersible On Oil Drilling Unit *Mater. Kompon. dan Konstr.*

[11] ASM International 2004 ASM Handbook Vol 9: Metallography and Microsctructures *ASM Int.*

[12] Devendranath Ramkumar K, Naren S V, Karthik Paga V R, Tiwari A and Arivazhagan N 2016 Development of pulsed current gas tungsten arc welding technique for dissimilar joints of marine grade alloys *J. Manuf. Process.*

[13] Marenych O and Kostryzhev A 2020 Strengthening mechanisms in nickel-copper alloys: A review *Metals (Basel).*

[14] ASTM 2015 B865-04 - Standard Specification for Precipitation Hardening Nickel-Copper-Aluminum Alloy (UNS N05500) Bar , Rod , Wire , Forgings , and

Forging Stock *Astm*
[15] ASTM Internaional 2012 ASTM E140-12b. Standard Hardness Conversion Tables for Metals Relationship Among Brinell Hardness, Vickers Hardness, Rockwell Hardness, Superficial Hardness, Knoop Hardness, Scleroscope Hardness, and Leeb Hardness *Am. Soc. Test. Mater.*
[16] Aminipour N and Derakhshandeh-Haghighi R 2019 The Effect of Weld Metal Composition on Microstructural and Mechanical Properties of Dissimilar Welds Between Monel 400 and Inconel 600 *J. Mater. Eng. Perform.*
[17] Special Metals Corporation 2000 *High-Performance Alloys for Resistance to Aqueous Corrosion*
[18] G. Budynas R and Nisbett J K 2017 *Shigley's Mechanical Engineering Design, 9th Edition-McGraw-Hill*